RSC Advances

This is an *Accepted Manuscript*, which has been through the Royal Society of Chemistry peer review process and has been accepted for publication.

Accepted Manuscripts are published online shortly after acceptance, before technical editing, formatting and proof reading. Using this free service, authors can make their results available to the community, in citable form, before we publish the edited article. This *Accepted Manuscript* will be replaced by the edited, formatted and paginated article as soon as this is available.

You can find more information about *Accepted Manuscripts* in the Information for Authors.

Please note that technical editing may introduce minor changes to the text and/or graphics, which may alter content. The journal's standard Terms & Conditions and the Ethical guidelines still apply. In no event shall the Royal Society of Chemistry be held responsible for any errors or omissions in this *Accepted Manuscript* or any consequences arising from the use of any information it contains.

ROYAL SOCIETY OF CHEMISTRY

www.rsc.org/advances

Improving the bias range for spin-filtering by selecting proper electrode materials

X. Q. Deng, * Z. H. Zhang, ** and C. H. Yang

Using the non-equilibrium Green's function method combined with the density function theory, we investigate the spin transport for carbon chain connected to electrodes with different materials. When carbon chain linked to C–H (C-H_2) bonded edge of H_2–ZGNR–H, the carbon chain displays a net spin polarization with a net magnetic moment of 1.367 μB (-0.935 μB) for C–H (C-H_2) bonded edge contact, but the direction of net magnetic moment is opposite, and the latter system shows a larger spin conductance. Then, we choose N-doping H_2–ZGNR–H as left electrode, and the right electrode is replaced by one caped carbon nanotube, armchair graphene nanoribbon (AGNR), and gold electrode, respectively. The conductance and the bias range for perfect spin-filtering of these systems show different obviously: carbon nanotube (Au) system shows weaker conductance, and AGNR system shows the largest bias range for perfect spin-filtering.

RSC Advances Accepted Manuscript

School of Physics and Electronic Science, Changsha University of Science and Technology, Changsha 410114, People's Republic of China. E-mail: xq_deng@163.com (X.Q. Deng), cscuzzh@163.com (Z.H. Zhang).Tel.: +86 0731 85258224; Fax: +86 0731 85258217

1. Introduction

Graphene nanoribbons (GNRs) derived from wafer-scale material are attractive candidates for next-generation integrated circuit.[1-4] In particular, the properties of GNR are strongly dependent on their chirality like carbon nanotubes.[5] Two particular types of GNRs with armchair and zigzag shaped edges have been extensively studied. Armchair graphene nanoribbons (AGNRs) are predicted to be metallic when $n=3m+2$, where n is the width and m is an integer, and are insulating otherwise.[6] Zigzag graphene nanoribbons (ZGNRs) are semiconducting with nonzero energy gaps due to the existence of ferromagnetically (FM) ordered edge states at each zigzag edge and an antiferromagnetic (AFM) arrangement of spins between two zigzag edges,[7] and there are peculiar localized electronic states at each edge,[8-11] which extend along the edge direction decay exponentially into the centre of the ribbon, with decay rates depending on their momentum. The localized edge states of the nonmagnetic case form two fold degenerate flat band at the Fermi energy (E_F), existing in about one-third of the Brillouin zone away from the zone centre.[12, 13] Kunstmann et al. consider that magnetic edge states might not exist in real systems for the intrinsic magnetism would not be stable at room temperature in GNRs.[14] Moreover, it has been estimated that the spin correlation length ξ limits the long-range magnetic order to 1nm at 300 K.[15] A feasible approach to realize graphene-based electronics is to construct the device junctions by connecting GNRs with different widths and orientations,[16] and giant magnetoresistance phenomen can be obtained by the application of an external magnetic field.[17] ZGNRs with asymmetric sp^2-sp^3 edges, however, exhibit an interesting bipolar magnetic semiconducting behavior, whose top valence bands and bottom conduction bands have opposite spin orientations in the proximity of the Fermi level,[18] and the composition of sp^2 and sp^3 types at the edges of the GNRs can be easily

RSC Advances Accepted Manuscript

controlled with experiment via temperature and pressure of H_2 gas. [19, 20] On the other hand, doping is a popular method to tune the properties of graphene.[21, 22] For instance, p-type or n-type doping graphene can serve as a promising anode electrode for high-power and high-energy lithium ion batteries under high-rate charge and discharge conditions, and the conductance of doping graphene is related with the doping element and position.[23-25] Spin-filtering effect is a particular phenomena in the spintronic device which is interesting topic due to its importance in next-generation electronics systems. [26] The range of bias for the spin-filtering effect, an important technique parameter for device, is narrow in current designed devices. For example, ZGNR-H/ZGNR-H2 heterostructure [27]shows the spin filter with bias range [0, 0.5] V, and ZGNR-H/ZGNR-O heterostructure[28] exhibits perfect spin-filtering when the bias is less than 0.2V. For carbon atomic chains coupled to ZGNR electrodes,[29] which is also a high-efficiency thermospin device,[30] displays perfect spin-filters under a small bias [-0.18, 0.18]V. Therefore, it is necessary to design some new devices with larger bias range for spin-filtering. As we all know, all the magnetism and electronic structure are directly related to the edge states for graphene. [31] H_2–ZGNR–H has two different edge states, C–H2 and C–H edge. In this paper, we first investigate spin transport features of a carbon chain linked to C–H (C-H_2) bonded edge of H_2–ZGNR–H with N-doping, which shows Half-metallicity. The perfect (100%) spin filtering effect can be obtained. Interestingly, the carbon chain displays a net spin polarization with a net magnetic moment of 1.367 μB (-0.935 μB) for the C–H (C-H_2) bonded edge contact, namely, the direction of net magnetic moments are anti-parallel, and the latter shows a larger conductance. Then, one electrode is replaced by one caped carbon nanotube, armchair graphene (AGNR), and Au (111), the spin filtering effect can still be obtained, but the conductance and the bias range for spin-filtering

RSC Advances Accepted Manuscript

change obviously.

2. Model and method

In our models as shown in Fig.1, the ribbon width of the H_2–ZGNR–H is characterized by the number of zigzag-shaped C chains, N_z, along the direction perpendicular to the nanoribbon axis, here $N_z = 6$, namely H_2–6ZGNR–H. For N-doping H_2–ZGNR–H, with N atom is doped near the C–H bonded edge, the nanoribbon is transformed to a half-metallicity irrespective of the ribbon width.[32] M1 and M2 are considered for carbon chain linked to C-H2 or C-H edge of H_2–6ZGNR–H, where carbon chain consists of seven carbon atoms. Then, by varying the right electrode materials and keeping the left electrode material (H_2–ZGNR–H) unchanged based on M2, we gain models M3, M4, and M5,where the right electrodes are one caped carbon nanotube, AGNR, and Au, respectively. Each device is composed of the left electrode, scattering region (the device region), and right electrode, marked by L, C, and R, respectively.

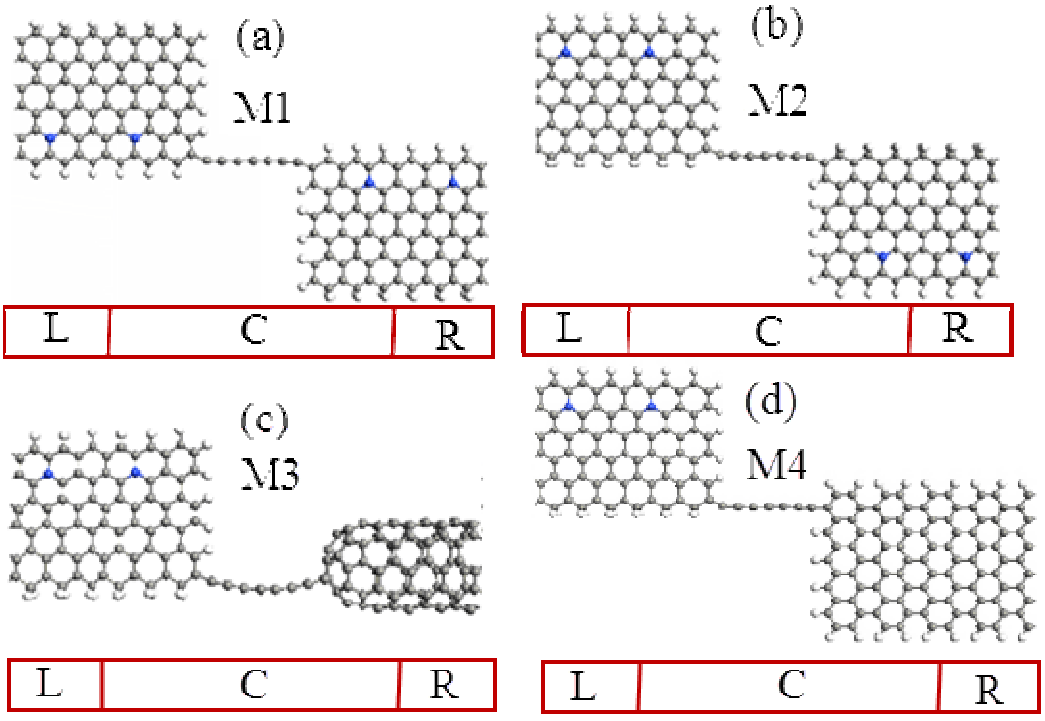

RSC Advances Accepted Manuscript

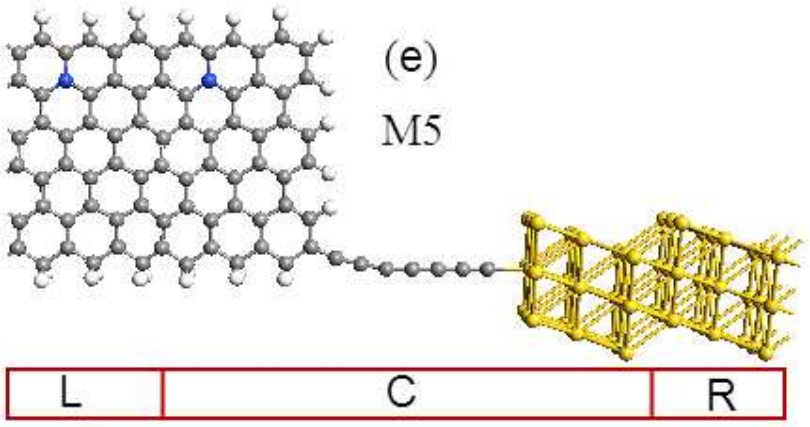

Fig.1. The geometric structures of M1~M5, the blue sphere denotes a doping N atom, the gray (white) sphere denotes the C (H) atom L, R, and C mean the left and right electrodes, and the central scattering region. The blue (gold) spheres denote doping N (Au) atom, the gray (white) spheres denote C (H) atom.

Geometries optimization and calculations of electronic structure are performed by using the spin-polarized density functional theory (DFT) combined with the non-equilibrium Green's function (NEGF) method as implemented in the Atomistix ToolKit11.8 (ATK11.8).[32] We employ Troullier-Martins norm-conserving pseudopotential to present the atom core and linear combinations of atom orbitals to expand the valence state of electrons. The local spin density approximation (LSDA) is used as the exchange-correlation functional. The real space grid techniques are used with the energy cutoff of 150 Ry as a required cutoff energy in numerical integrations and the solution of Poisson equation using fast fourier transform (FFT). The k-point sampling is 1, 1, and 100 in the x, y, z direction, respectively, where z is the electronic transport one. Open boundary conditions are used to describe the electronic and the transport properties of nanojunctions. The geometrical structures used are optimized until all residual forces on each atom are smaller than 0.05 eV/Å under the periodic boundary condition. The wave functions of C and H atoms are expanded by single-zeta polarized (SZP) basis set. The current I_σ in systems as a function of the applied external bias V_b, can be calculated from the Landauer-like formula, [33]

$$I_\sigma(V_b) = (e/h)\int_{\mu_r(V_b)}^{\mu_l(V_b)} T_\sigma(E,V_b)[f_l(E,V_b) - f_r(E,V_b)]dE \quad (1)$$

where $\sigma = \uparrow$ (spin up) and $\downarrow$ (spin down), $T_\sigma(E,V_b)$ is the bias-dependent transmission

RSC Advances Accepted Manuscript

coefficient, $f_{l/r}(E,V_b)$ is the Fermi–Dirac distribution function of the left (right) electrode, As a result, the electrochemical potentials correspond to $\mu_l(V_b)=\mu_l(0)-eV_b/2$ and $\mu_r(V_b)=\mu_r(0)+eV_b/2$, when the external bias is V_b. Consider the fact that the Fermi level is set to be zero, the region of the energy integral window [$\mu_l(V_b)$, $\mu_r(V_b)$] can be written as [$-V_b$ /2, V_b/2].

3. Results and discussion

At First, we discuss the edge-state effects for the carbon chain linked to C-H2 or C-H edge of H_2–6ZGNR–H, as M1 and M2. The $I-V$ curves at various biases are shown in Fig.2 (a), and the distinct features are as follows: the current for α - spin state is completely suppressed, while the current for β - spin component is obvious lager than that for the α-spin state, and the corresponding spin polarization, $|(I_\alpha - I_\beta)/(I_\alpha + I_\beta)|$, reaches 100% when the bias is below 0.9V. Moreover, the negative differential resistance (NDR) behaviors also can be obtained, which is described by a decrease in current through the system with the steady increase in applied bias. We also can see that the current in M1 is smaller than that of M2, and NDR phenomenon is also weak. Interestingly, from the Fig. 2 (b), we can see that the net spin magnetism exists in carbon chains with an alternate emergence of the stronger β -spin and weaker α-spin in M1, with a net magnetic moment of 1.367 μB, while the carbon chain almost exhibits an alternate emergence of the stronger α-spin and weaker β-spin in M2 with a net magnetic moment of -0.935 μB, seen in Fig. 2 (c), which means the direction of two net magnetic moments is opposite for M1 and M2. The polarization in the A sublattice is much stronger than that in the B sublattice, and the spin direction of A and B sublattices is antiparallel indicating negative exchange interactions between the nearest neighbor atoms. The stronger magnetism can be found at the dihydrogen, and a weak magnetism can be observed on the carbon atom with dihydrogen termination, while the atoms next to them feature a stronger spin polarization because it decays much more slowly to the center due to the different localization in the edge states. It can be seen that the local magnetization at the doping sites and their vicinity is strongly suppressed, giving rise to the decrease of net magnetic moment of the whole system. Since nitrogen has one electron more than carbon,

RSC Advances Accepted Manuscript

which is injected to the device after its substitutional doping. Thus the Fermi energy is pushed up slightly into the conduction band, and some α – spin states are occupied, thereby causing a decrease of the net magnetic moment of the device. The current is determined by the integral area of transmission curve within the bias window. In Fig.3 (a) and (b), we show the spin-dependent transmission spectrum for M1 and M2 at 0.5V, respectively. The main transmission peaks including the β-spin HOMO (highest occupied molecular orbital) peak and β-spin LUMO (Lowest unoccupied molecular orbital) peak near the Fermi level within the bias windows, so the α-spin current is nearly zero, and spin-filter effects can be achieved. To provide an insight into the spin-filter behavior, we investigate the spatially resolved local density of states (LDOS) at Fermi level under 0.5V, shown in Fig. 3 (c) and (d). The LDOS is localized at the right electrode and partly distribute on the carbon chain for M1, but is highly delocalized throughout the scattering region and possess significant values on the carbon chain. It is evident that the LDOS for M1 is much higher than that of M2. We further calculate the electron transmission pathways for at energy point of transmission peak, which is an analysis option which splits the transmission coefficient into local bond contributions. The pathways have the property that if the system is divided into 2 parts (A, B), then the pathways across the boundary between A and B sum up to the total transmission coefficient: $T(E) = \sum_{i \in A, j \in B} T_{ij}(E)$. Usually, the primary use for the pathways is to figure out where (and how) the current propagates, the more arrows, the more transmission .[34, 35] Fig.3 (e) shows the transmission pathways of β– spin at Fermi energy under 0.5 V for M1, we can see that the local currents (from the left to the right) is nearly zero in the devices, for the electrons of left electrode can not reach the right one. While for M2, seen in Fig.3 (f), stronger local currents can transmit from left electrode to the right one via the carbon chain.

RSC Advances Accepted Manuscript

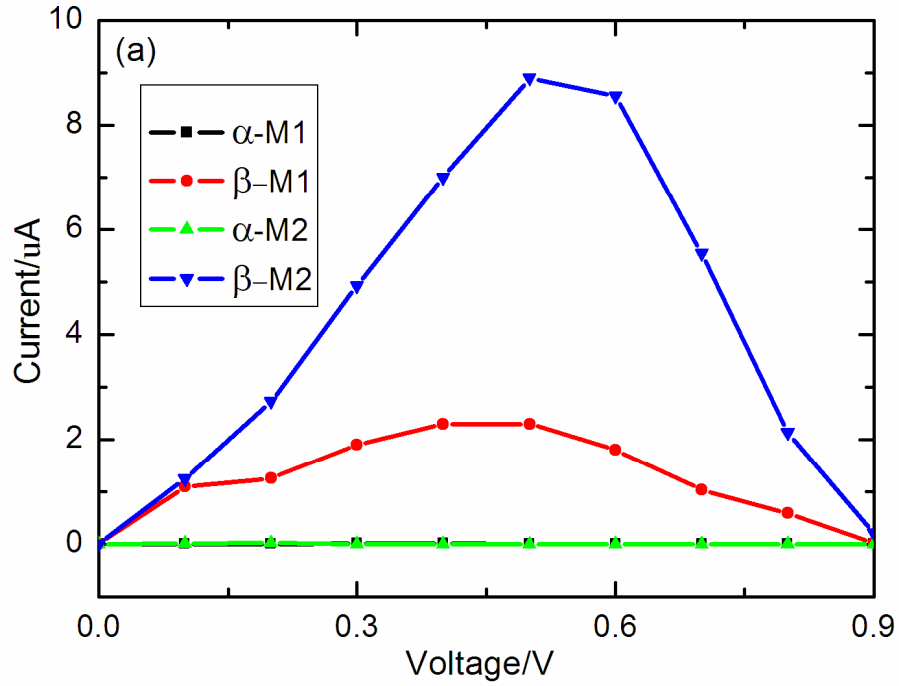

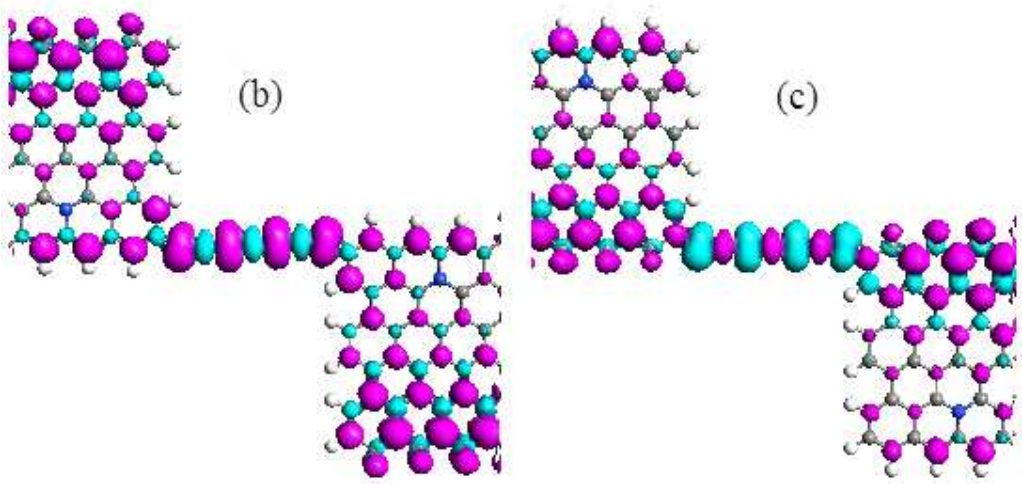

Fig 2. The spin-dependent $I - V$ curves for M1 and M2; (b) and (c) spin density for M1 and M2 under zero bias. The magenta and cyan colors stand for the β-spin and α-spin components, respectively. The isosurface level is taken as 0.01 e/Å^3

RSC Advances Accepted Manuscript

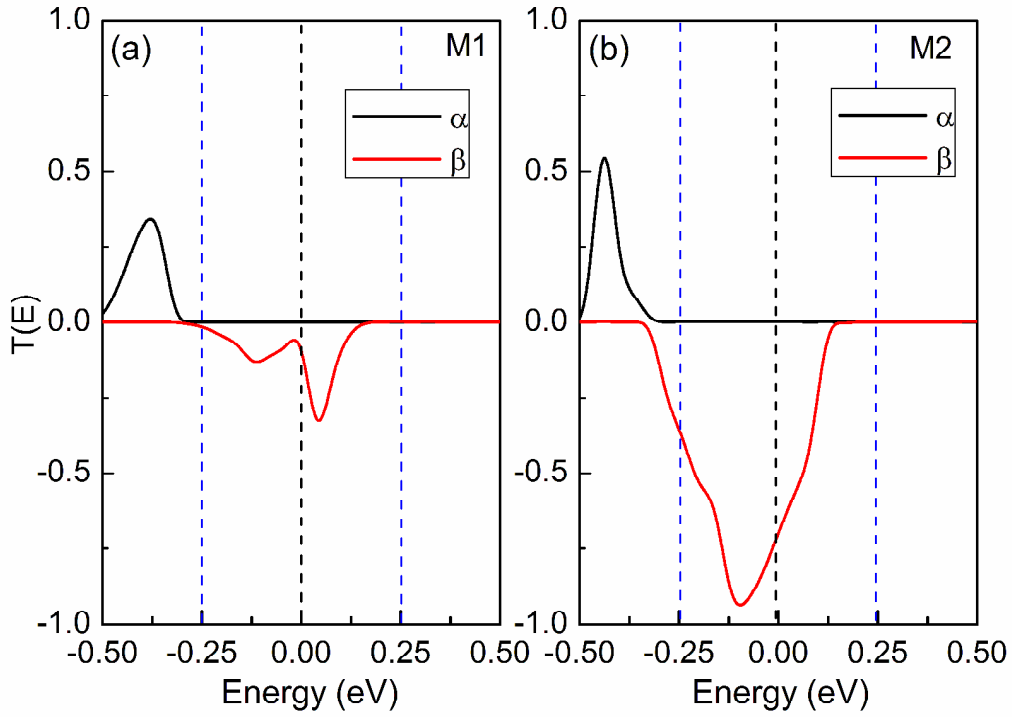

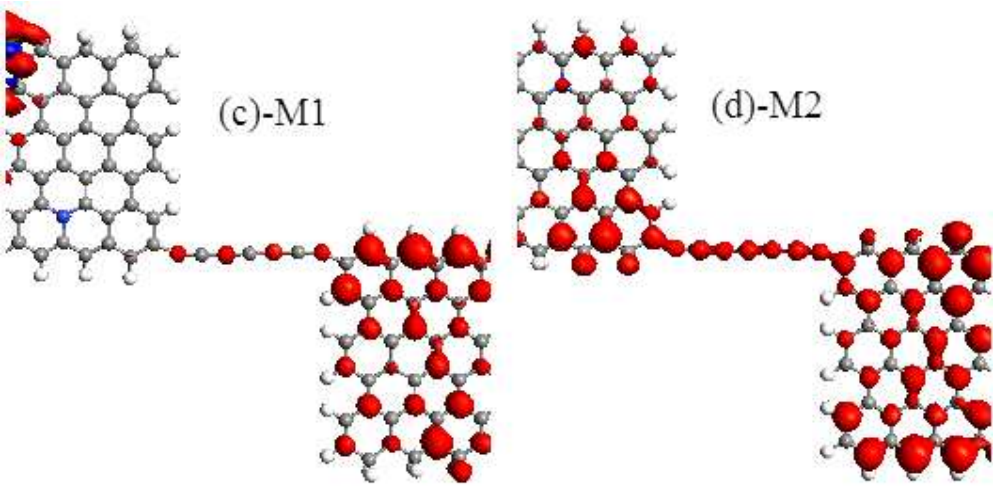

RSC Advances Accepted Manuscript

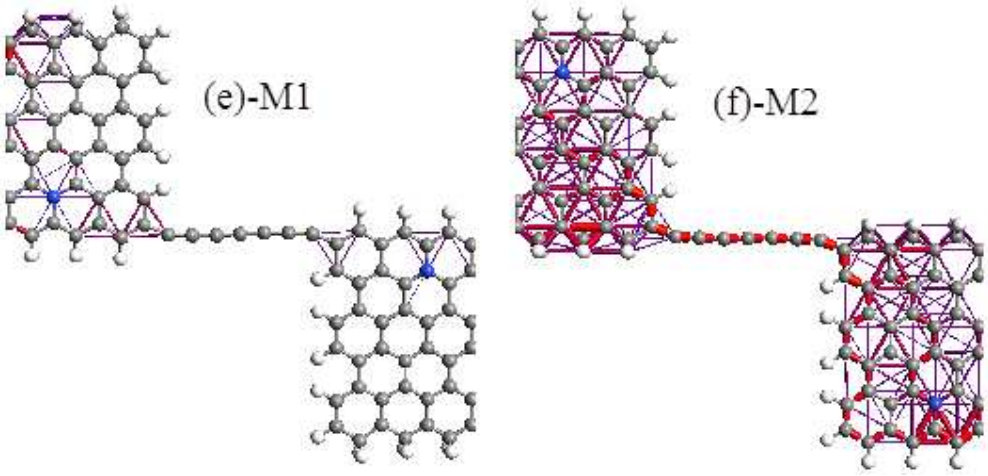

Fig 3. (a)The transmission spectra, (c) the LDOS and (e) local currents transmission pathway at Fermi energy at 0.5V for M1, (b), (d) and (f) the same for M2. The blue dotted lines denote the chemical potentials of left and right electrodes, and the Fermi level is set to zero.

Next, the right electrode is replaced by one caped carbon nanotube (the cap is derived from half of a C60 molecule) based on M2, and this model are denoted as M3. The $I - V$ curves at various biases are shown in Fig.4 (a): the current for β - spin component is obvious lager than that for the α-spin state, which is completely suppressed, and spin polarization reaches 100% between zero and 1.0V bias. However, the current of M3 shows a smaller value obviously than that of M1 and M2. Isosurface plots of the spin charge density difference of α-and β-spin states for M3 is shown in the inset of Fig.4 (a), and the net spin magnetic moment exists in a carbon chain with an alternate emergence of the stronger α-spin is -1.046 μB. To find the origin for weak current, electrostatic potential [36] distribution is shown in Fig.4 (b): the potential profile is asymmetric on the interface between a carbon atom chain and two electrodes, and two tunnel barriers at both interfaces are formed, and the right barrier is higher than the left one, which makes the electrons move difficultly under bias. In Fig.4 (c), we give β-spin transmission spectra and molecular energy level in the scattering region at 0.5V for M3. Besides, we also plot the MPSH of HOMO and LUMO for β-spin within bias window. As can be seen that the main transmission peaks including the β-spin HOMO and LUMO peaks are near the Fermi level within the bias windows. The magnitude of transmission coefficients is

RSC Advances Accepted Manuscript

related to the number of the molecular orbital and the delocalization degree of the molecular orbital. It can be found that there are two molecular orbitals appearing in the bias window indicated between black dashed lines, and spatial distributions of the molecular projected self-consistent Hamiltonian (MPSH) show that the HOMO and LUMO are localized, which lead to a weaker electronic transmission capability. The HOMO state distributes largely on the left electrode and carbon chain, and nearly no distribution on the right electrode. While for LUMO state, it shows much distribution on the right electrode and carbon chain, and no distribution on the graphene electrode.

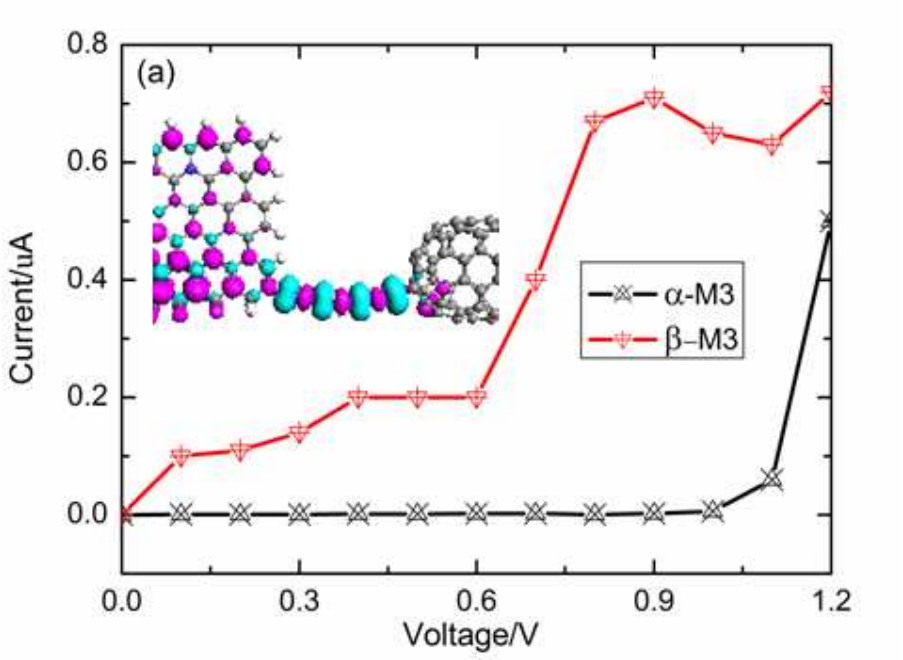

RSC Advances Accepted Manuscript

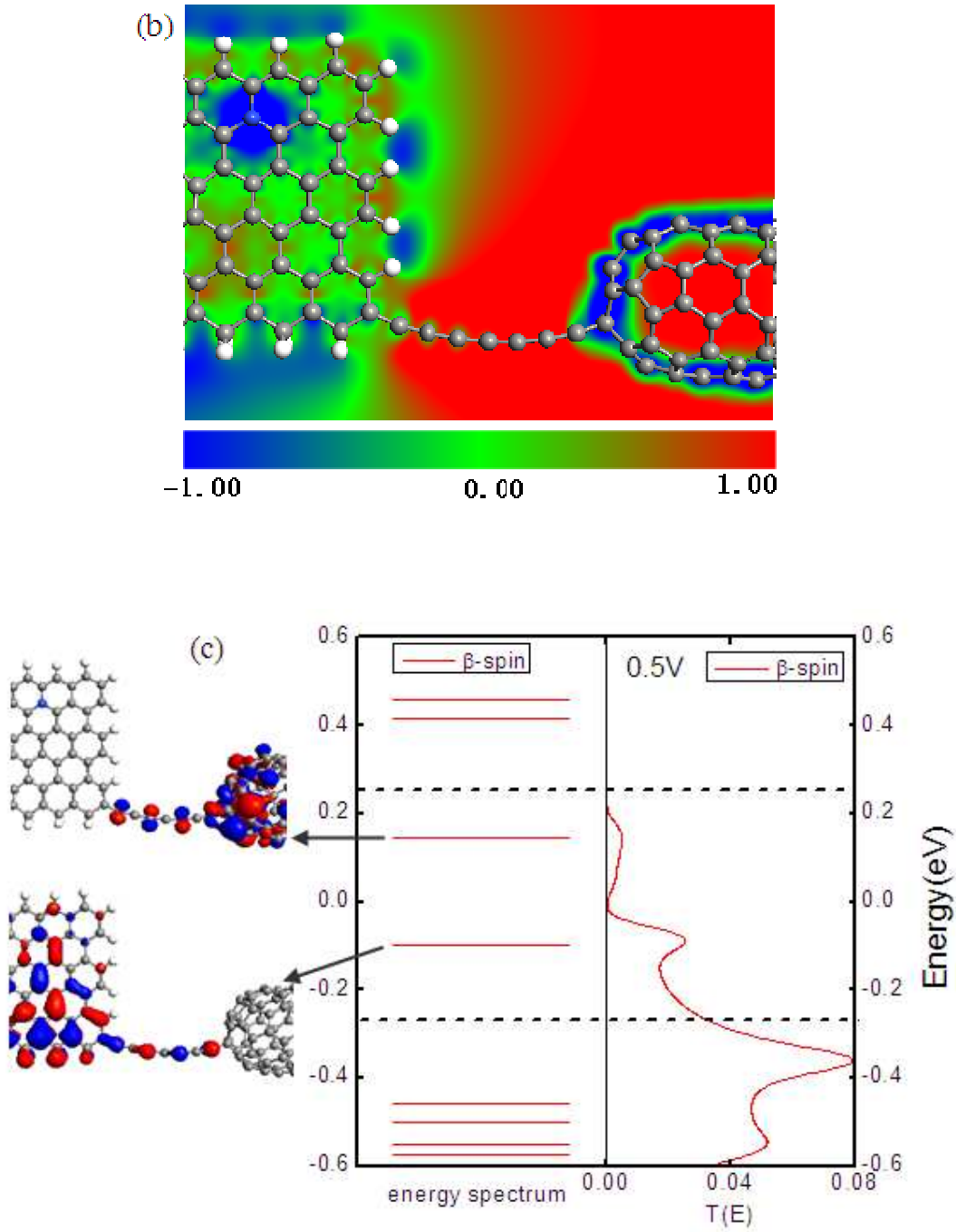

Fig.4. (a) the spin-dependent $I - V$ curves for M3, and the inert is spin density, (b) the electrostatic potential distribution, and (c) β-spin molecular energy level spectra and transmission curves in scattering region for M3. The dashed black lines represent the bias window. The Fermi level is set at zero. The left region of each figure gives the MPSH of HOMO and LUMO.

When the right electrode is replaced by armchair graphene with width n=11, based on

RSC Advances Accepted Manuscript

M2, and this model are denoted as M4. The $I - V$ curves at various biases are shown in Fig.5(a), the obvious spin polarization can be seen in the bias range [0, 1.2]V, for the for α - spin current is completely suppressed which less than the β - spin component with large magnitude, spin polarization reach 100% in the bias range[0, 1]V, and 86% in the bias range[1.1, 1.2]V. Isosurface plots of the spin charge density difference of α-and β-spin states for M4 is shown in the inset of Fig.5 (a), and the net spin magnetic moment of carbon chain is -1.137 μB. To explain the spin polarization, we give the band structure for the left (right) electrode, transmission at 0.8V, shown in Fig. 5(b). The horizontal dashed lines denote the chemical potentials of left and right electrodes. The energy bands are shifted downward and upward for the left and right electrodes under positive bias, respectively. Within the bias window, the α-spin band for both of the left and right electrode have no overlaps, and no α-spin current, for the β-spin band of left electrode overlaps with that of right electrode, therefore the β-spin transmission peaks can be obtained. As a contrast, we also give the plot at the same bias for M2, shown in Fig. 5(c). Only one narrow β-spin transmission peak appears in the window for such a little overlaps of the β-spin band between left and right electrode, which lead to weaker current compared with M4. Then, with the increase bias, the energy bands are further shifted downward and upward for the left and right electrodes, the overlaps will decrease and the currents also become weaker and weaker accordingly.

RSC Advances Accepted Manuscript

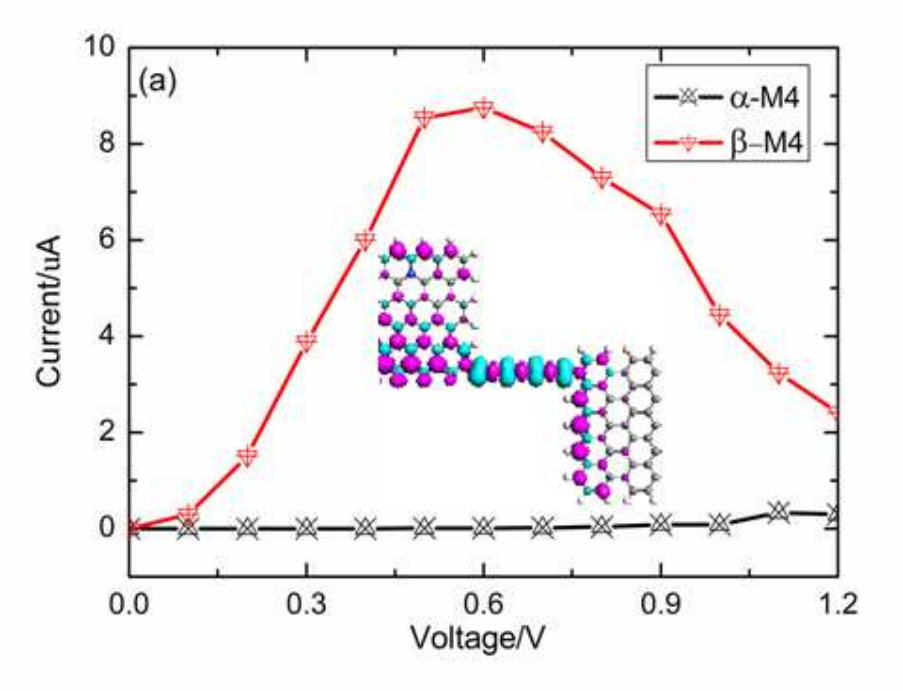

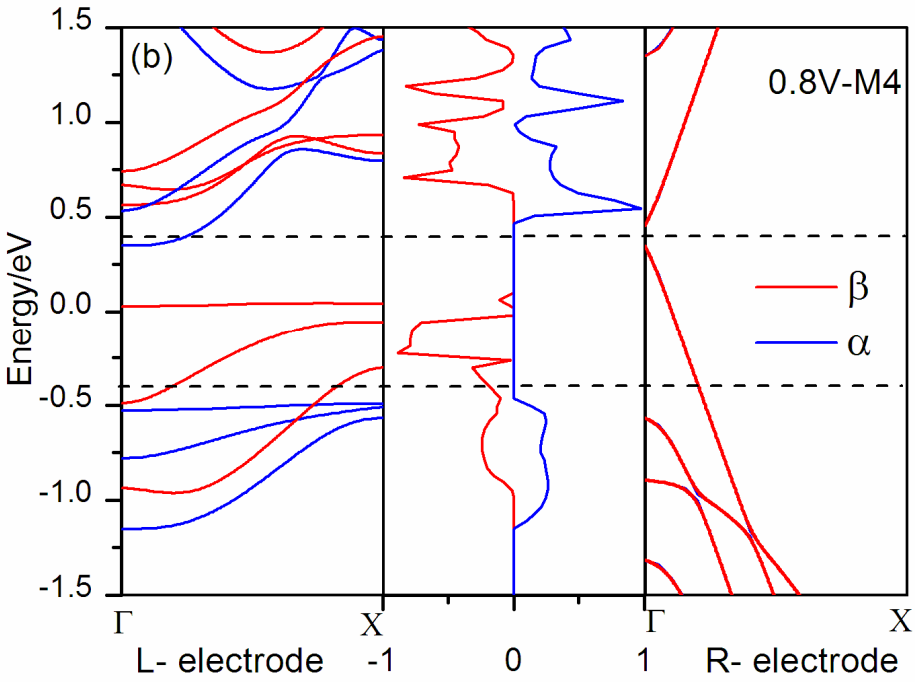

RSC Advances Accepted Manuscript

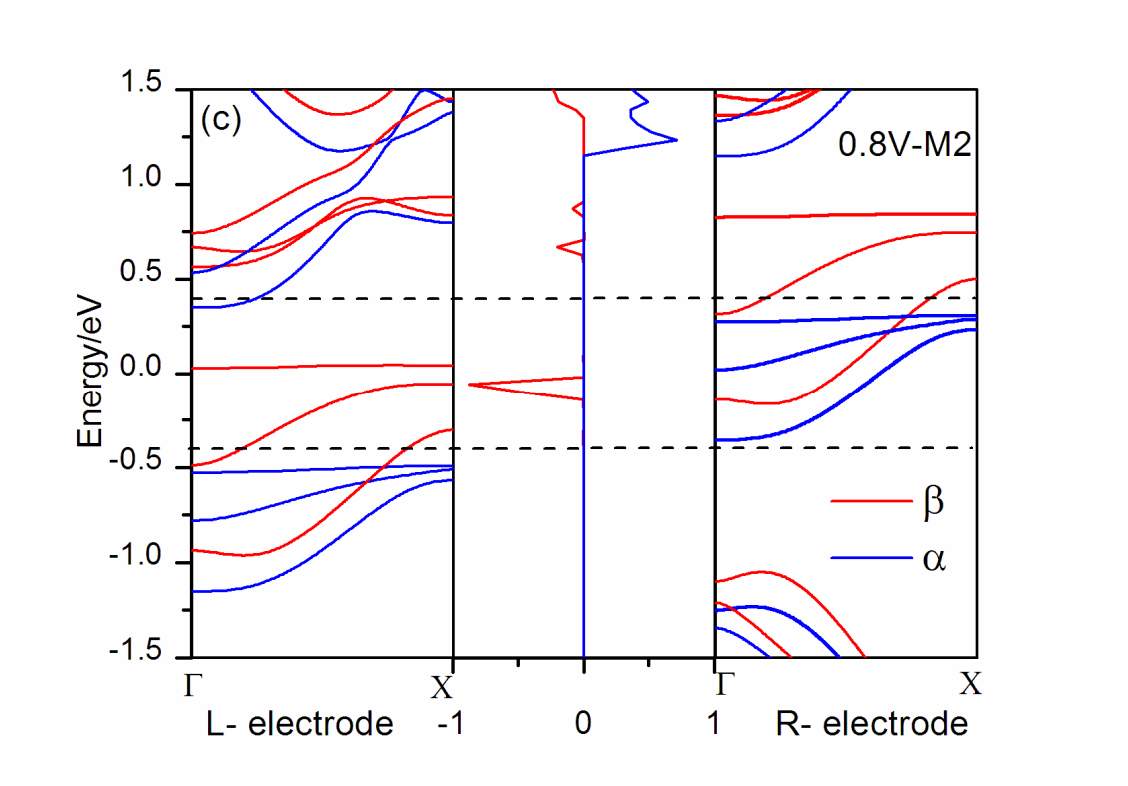

Fig.5 (a) the spin-dependent *I* – *V* curves for M4, the inert is spin density, band structure for the left electrode, transmission spectrum, and band structure for the right electrode at FM state under 0.8V bias (b) for M4 and (c) for M2, the dashed black lines represent the bias window.

At last, the right electrode is replaced by semi-infinite Au (111) based on M2, with the surface consists of 3 × 3 Au atoms, we obtained M5. The *I* – *V* curves at various biases are shown in Fig.6 (a), the obvious spin polarization only occurs in the bias range [0, 0.8]V, and the β - spin currents show small magnitude which like as M3. The net spin magnetic moment of carbon chain is -1.124 μB which shown in. the inset of Fig.6 (a). To understand the origin of weak current, we plot the transmission spectrum and the electrostatic potential distribution.at zero bias, shown in Fig.6 (b). One obvious barrier appears at the interface between carbon chain and Au electrode, which hinder the movement of electrons. The α - spin transmission coefficient is zero near the Fermi energy, but one obvious β - spin transmission peak emerge at Fermi energy, and the coefficient is around 0.15 which lead to the weak β –

RSC Advances Accepted Manuscript

spin current under low bias.

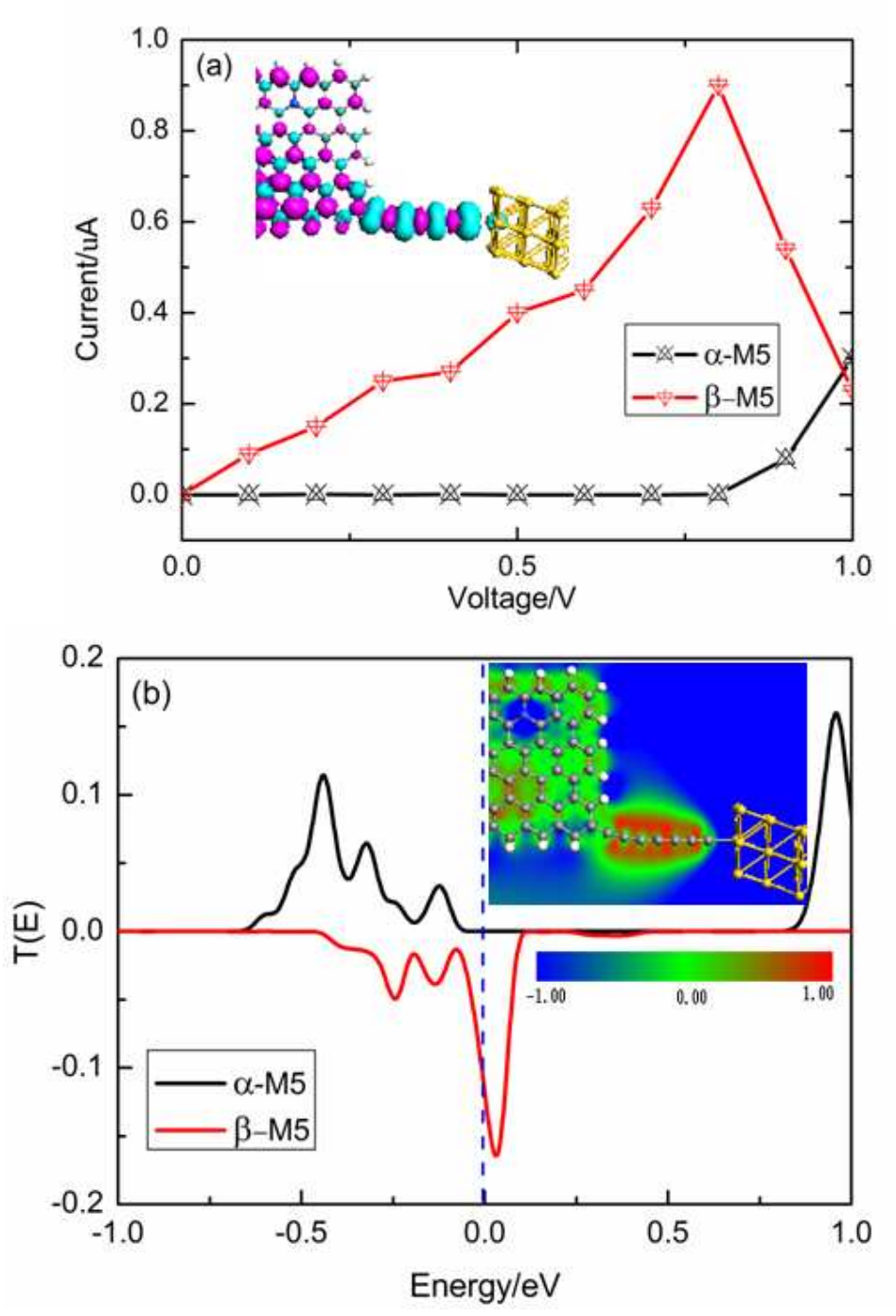

Fig.6. (a) the spin-dependent *I* – *V* curves, and the inert is spin density, (b) transmission spectrum under zero bias for M5, the inert is the electrostatic potential distribution.

RSC Advances Accepted Manuscript

4. Conclusion

In summary, the spin transport for carbon chain connected to electrodes with different materials are investigated by the non-equilibrium Green's function method combined with the density function theory. We first investigate spin transport features of a carbon chain linked to C–H (C-H_2) bonded edge of H_2–ZGNR–H. Interestingly, the carbon chain displays a net spin polarization with a net magnetic moment of 1.367 μB (-0.935 μB) for C–H (C-H_2) bonded edge contact, but the direction of net magnetic moments is opposite, the latter device has a larger spin conductance. Then, we choose N-doping H_2–ZGNR–H as left electrode, and the right electrode is replaced by one caped carbon nanotube, armchair graphene nanoribbon (AGNR), and gold electrode, respectively. The conductance and the bias range for perfect spin-filtering of these systems show different obviously, and carbon nanotube (Au) system shows weaker conductance, AGNR system shows the largest bias range for perfect spin-filtering.

Acknowledgments

This work was supported by the National Natural Science Foundation of China (Grant Nos. 61371065 and 61201080), the Hunan Provincial Natural Science Foundation of China (Grant No 2015JJ3002), the Construct Program of the Key Discipline in Hunan Province, and Aid Program for Science and Technology Innovative Research Team in Higher Educational Institutions of Hunan Province.

References

1 K. S. Novoselov, A. K. Geim, S. V. Morozov, D. Jiang, Y. Zhang, S. V. Dubonos, I. V. Grigorieva and A. A. Firsov, Science, 2004, 306, 666.

2 K. S. Novoselov, A. K. Geim, S. V. Morozov, D. Jiang, M. I. Katsnelson, I. V. Grigorieva, S. V. Dubonos and A. A. Firsov, Nature (London), 2005, 438, 197.

3 Y. Zhang, Y.-W. Tan, H. L. Stormer, and Philip Kim, Nature (London), 2005, 438, 201.

RSC Advances Accepted Manuscript

4 J. M .Zheng, P. Guo, Z. Ren, Z. Jiang, J. Bai, Z. Zhang , Appl. Phys. Lett., 2012, 101, 083101.

5 Z. H. Zhang, J. Peng and H. Zhang, Appl. Phys. Lett. 2001,79, 3515; Z. H. Zhang, J. Peng and X. Huang, Phys. Rev. B, 2002, 66, 085405; Z. H. Zhang, Z. Yang and X. Wang, J. Phys: Condens Mat., 2005, 17, 4111.

6 Y.-W. Son, M. L. Cohen, and S. G. Louie, Phys. Rev. Lett. 2006, 9, 216803.

7 T. Ozaki, K. Nishio, H. Weng, and H. Kino, Phys. Rev. B., 2010, 81, 075422.

8 H. Lee, Y. Son, N. Park, S. Han, and J. Yu, Phys. Rev. B, 2005, 72, 174431.

9 H. Şahin and R. T. Senger, Phys. Rev. B, 2008, 78, 205423.

10 Z. F. Wang,, Shuo Jin, and Feng Liu, Phys. Rev. Lett., 2013,111, 096803.

11 C. Cao, L. Chen, M. Q. Long, W.R. Huang, and H. Xu, J. Appl. Phys., 2012, 111, 113708.

12 L.Shen, M Zeng, S. Li, M. B. Sullivan, Y. P. Feng, Phys. Rev. B, 2012, 86, 115419.

13 X. H. Zheng, X. L. Wang, L. F. Huang, H. Hao, J. Lan, Z. Zeng, Phys. Rev. B, 2012, 86, 081408.

14 J. Kunstmann, C. Özdoğan, A. Quandt, and H. Fehske, Phys. Rev. B, 2011, 83, 045414.

15 O. V. Yazyev, and M. I. Katsnelson, Phys. Rev. Lett., 2008, 100, 047209.

16 D. A. Areshkin, and C. T. White, Nano Lett., 2007, 7, 3253.

17 F. Muñoz-Rojas, J. Fernández-Rossier, and J.J. Palacios, Phys. Rev. Lett., 2009, 102,136810.

18 J. Kang, F. M. Wu, J. B. Li, Appl. Phys. Lett., 2011, 98, 083109.

19 Y. H. Lu, R. Q. Wu, L. Shen, M. Yang, Z. D. Sha, Y. Q. Cai, P. M. He, Y. P. Feng, Appl. Phys. Lett. 2009, 94 122111.

20 B. Xu, J. Yin, Y. D. Xia, X. G. Wan, K. Jiang,and Z. G.. Liu, Appl. Phys. Lett., 2010, 96 163102.

21 Z. F. Wu, W. C. Ren, L. Xu, F. Li and H. M. Cheng, ACS Nano, 2011, 5, 5463.

22 W. Sheng, Z. Y. Ning2, Z. Q. Yang and H. Guo, Nanotechnology, 2010, 21, 385201.

23 D. J. Late, A. Ghosh, K. S. Subrahmanyam, L. S. Panchakarla,S. B. Krupanidhi, and C. N. R. Rao, Solid State Commun., 2010, 150, 734.

24Y. An, X. Wei and Z. Yang, Phys. Chem. Chem. Phys. 2012, 14, 15802.

25X. H. Zheng, X. L. Wang, T. A. Abtew, and Z. Zeng J. Phys. Chem. C, 2010,114, 4190.

26 X. F. Yang, Y. S. Liu, X. Zhang, L. P. Zhou, X. F. Wang, F. Chi, J. F. Feng, Phys. Chem. Chem. Phys., 2014, 16, 11349.

RSC Advances Accepted Manuscript

27 J. Zeng, K. Q. Chen, J. He, X. J Zhang, C. Q. Sun, J Phys Chem C, 2011, 115, 25072.

28 M. G. Zeng, L.Shen, M. Yang, C. Zhang, Y. P. Feng, Appl. Phys. Lett., 2011, 98, 053101.

29 M. G. Zeng, L.Shen, Y. Q. Cai, Z. D. Sha, Y. P. Feng Appl. Phys. Lett., 2010, 96, 042104.

30 Y. S. Liu, X. Zhang, J. F. Feng, X. F. Wang, Appl. Phys. Lett., 2014, 104,242412

31E. Kan, Z. Li, J.Yang and J. G. Hou, J. Am. Chem. Soc., 2008, 130, 4224.

32 X. Deng, Z. Zhang, G. Tang, Z. Fan, H. Zhu, C. Yang, Sci. Rep., 2014, 4, 4038

33M. Buttiker and R. Landauer, Phys. Rev. B, 1985, 31, 6207.

34 G. C. Solomon, C. Herrmann, V. Mujica, M. A. Ratner, Nat. Chem. 2010, 2, 223.

35 A. H. Castro Neto, F. Guinea, N. M. R. Peres, K. S. Novoselov, A. K. Geim, Rev. Mod. Phys., 2009, 81, 109.

36 J. B. Pan, Z. H. Zhang, K. H. Ding, X. Q. Deng, and C. Guo, Appl. Phys. Lett., 2011, 98, 092102.

RSC Advances Accepted Manuscript